PHYSICAL REVIEW C VOLUME 25, NUMBER 1 JANUARY 1982

Quantum calculation of the barrier and internal wave contributions to light- and heavy-ion elastic scattering

J. Albiński* and F. Michel
Faculté des Sciences, Université de l'Etat, B-7000 Mons, Belgium
(Received 3 August 1981)

We propose a new technique allowing the decomposition of the light- and heavy-ion elastic scattering amplitude into its barrier and internal wave components as defined by Brink and Takigawa. The method requires only minimum programming as it makes use of the reflection coefficients generated by any optical model code. Also, it can be applied to a wide range of potentials including folding model and model-independent potentials. The use and physical interest of the method are illustrated by applying it to a few representative examples ranging from α to heavy-ion scattering.

[NUCLEAR REACTIONS Calculation of barrier and internal wave components of elastic scattering amplitude; application to light- and heavy-ion scattering.]

I. INTRODUCTION

Semiclassical methods have often played a key role in elucidating the mechanism of light- and heavy-ion scattering (see, e.g., Ref. 1 and references therein). In particular, they help to disentangle the various ingredients of the scattering amplitude in an intuitively appealing way. Recently Brink and Takigawa have extended the semiclassical solution of the three turning point scattering problem to the case of complex potentials.[2] Their method not only leads to a good agreement with full quantum calculations, but also allows them to separate the elastic scattering amplitude into two parts; the "barrier contribution" corresponding to the wave reflected at the barrier of the effective potential, and the "internal contribution" originating from the wave passing the barrier and reflected at the most internal turning point.

Although their method provides valuable information on the physics underlying the optical model description of the scattering, it has up to now been applied to a rather limited number of cases, probably because of the difficulties inherent to its programming. Moreover, the method requires the potential to be supplied as a single analytical expression, which makes it inapplicable to a wide range of currently used interactions (e.g., folding model and most of the so-called "model-independent" potentials). This prompted us to investigate the possibility of gaining the same physical information without resorting to a full semiclassical calculation. In this spirit we have developed an algorithm requiring simple modifications of any conventional optical model code and leading to a very good agreement with the semiclassical method.

In Sec. II we recall briefly the assumptions and main formulas of Brink and Takigawa's model and we present the principles of our approach. Section III is devoted to a discussion of its practical aspects, while Sec. IV deals with its application to a few illustrative examples ranging from alpha- to heavy-ion scattering. A brief summary and our conclusions are presented in Sec. V.

II. DECOMPOSITION OF THE ELASTIC SCATTERING AMPLITUDE INTO ITS BARRIER AND INTERNAL WAVE CONTRIBUTIONS

Given an optical potential

$$U(r)=V(r)+iW(r) \tag{1}$$

we define the effective potential U_{eff} corresponding to angular momentum l by

$$U_{\text{eff}}(r)=V_{\text{eff}}(r)+iW(r)\ , \tag{2}$$

where

$$V_{\text{eff}}(r)=V(r)+V_C(r)+\frac{\hbar^2}{2\mu}\frac{l(l+1)}{r^2}\ , \tag{3}$$

V_C denotes the Coulomb potential, and μ is the reduced mass of the system (here and in the following, the angular momentum index will be consistently dropped if not needed). If the real part of the nuclear interaction is deep enough, then V_{eff} displays a "pocket" (cf. Fig.1). When $W=0$ and $E_{\text{c.m.}}$ is less than the barrier height V_B there are three real semiclassical turning points, corresponding to $V_{\text{eff}}-E_{\text{c.m.}}=0$. These move into the complex plane when $W\neq 0$ and/or $E_{\text{c.m.}} > V_B$. A configuration of the turning points corresponding to $W<0$ is displayed schematically in Fig. 2.

Provided that the two outer turning points 1 and 2 are well separated from the inner one (i.e., that V_{eff} has a well marked pocket), the reflection coefficient η can be written as[2]

$$\eta \equiv e^{2i\delta} = \frac{e^{2i\delta_1}}{N} + \frac{e^{2i\delta_3}}{N(N+e^{2iS_{32}})} . \tag{4}$$

δ_1 is the WKB phase shift corresponding to the external turning point 1. The phase shift δ_3 corresponding to the internal turning point 3 can be written as

$$\delta_3 = S_{32} + S_{21} + \delta_1 . \tag{5}$$

N is connected to the barrier penetrability, and the S_{ij} are semiclassical action integrals evaluated in the complex plane

$$S_{ij} = \int_{r_i}^{r_j} \left\{ \frac{2\mu}{\hbar^2} [E_{\text{c.m.}} - U_{\text{eff}}(r)] \right\}^{1/2} . \tag{6}$$

In most cases absorption is strong enough to make the imaginary part of S_{32} large and to allow (4) to be approximated as[2]

$$\eta \approx \frac{e^{2i\delta_1}}{N} + \frac{e^{2i\delta_3}}{N^2} \equiv \eta_B + \eta_I . \tag{7}$$

η_B and η_I can be interpreted as corresponding to the wave reflected at the barrier (i.e., turning point 1) and to that reflected once at the most internal turning point 3. Approximation (7) amounts to a complete neglect of multiple reflection between points 2 and 3. The corresponding scattering amplitudes f_B and f_I are defined in terms of $\eta_B(l)$ and $\eta_I(l)$ as

$$f_B(\theta) = \frac{1}{2ik} \sum_l (2l+1) e^{2i\sigma_l} [\eta_B(l) - 1] \times P_l(\cos\theta) + f_c(\theta) , \tag{8}$$

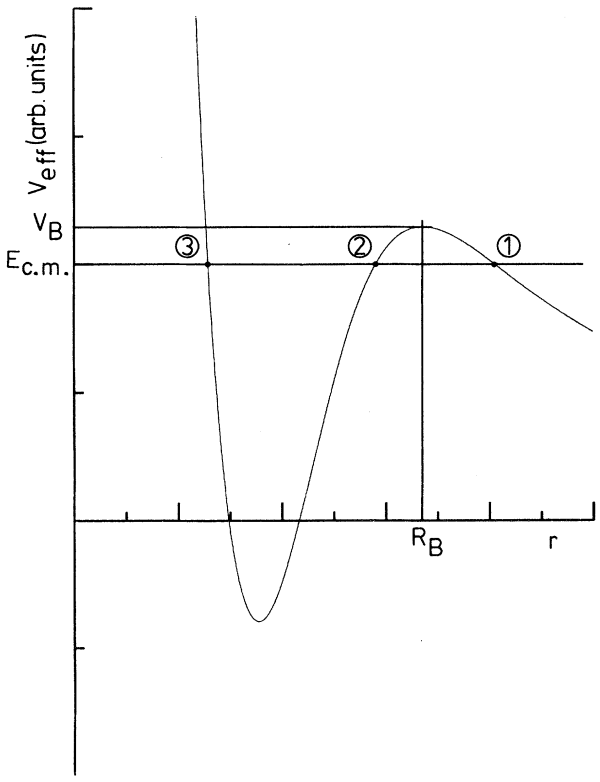

FIG. 1. Schematic representation of the effective potential for a particular l value in the case of a deep real potential.

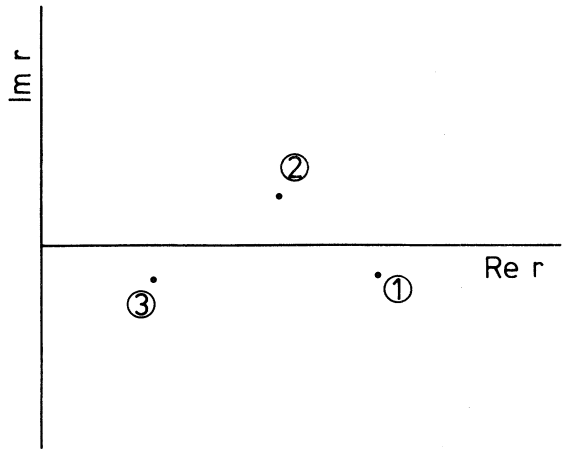

FIG. 2. Location of the turning points in the complex plane for a particular l value for $W<0$ and $E_{\text{c.m.}} > V_B$ (schematic) (cf. Ref. 2).

$$f_I(\theta)=\frac{1}{2ik}\sum_l (2l+1)e^{2i\sigma_l}\eta_I(l) \times P_l(\cos\theta) , \quad (9)$$

in the usual notation. The total elastic scattering amplitude f reads in approximation (7)

$$f(\theta)\approx f_B(\theta)+f_I(\theta) . \quad (10)$$

Brink and Takigawa were able within their semiclassical approach to obtain a good agreement with full quantum calculations. However, their method requires the localization of the complex turning points and the evaluation of several action integrals in the complex plane, making its practical use rather difficult. Also, it is restricted to analytical potentials and thus does not allow for direct investigation of the interesting cases of folding model, spline, and Fourier-Bessel, and in general, numerically-supplied potentials.

We therefore tried to develop a more flexible method, based on simple modifications of any optical model code. In order to test our method we compared our calculations of reflection coefficients and scattering amplitudes for several representative examples with those generated by a WKB code[3] written within the frame of Brink and Takigawa's approach.

First, we attempted to eliminate the internal wave contribution by artifically enhancing the absorption inside the potential pocket, so that only the barrier wave contribution survives. The internal part can be calculated thereafter by substracting the barrier part from the full scattering amplitude. A similar approach has been used independently by Rowley *et al.*[4] in the case of $^{12}C+^{12}C$ scattering. Although it gives a good agreement with WKB in most cases, sometimes it was found to lead to serious discrepancy with the semiclassical calculation. The essential reason of the failure seems to be that the extra absorptive potential must be very strong to completely suppress the internal wave, yet its contribution at the barrier must be negligible not to affect the barrier part of the scattered wave. This forces the use of a very abrupt modification of the imaginary potential, which in some cases introduces an additional turning point, i.e., causes unwanted extra reflection.

In order to avoid these difficulties we searched for an alternative method requiring less drastic modifications of the interaction potential and based on a better understanding of their influence on the scattering reflection coefficients. Brink and Takigawa[2] pointed out that the modulus of the s-wave internal reflection coefficient for $^{40}Ca(\alpha,\alpha)$ scattering at 29 MeV incident energy behave exponentially as a function of absorption. In fact it can be shown on general grounds that a complex perturbation of the interaction potential

$$U_{\rm eff}(r)\rightarrow U_{\rm eff}(r)+\kappa g(r) , \quad (11)$$

[where κ is a complex factor and g(r) some analytical complex function] causes a modification of the action integrals (taken between turning points r_i and r_j) linear to first order in κ

$$S\rightarrow S+\alpha\kappa , \quad (12)$$

where α is a complex constant given by

$$\alpha=\left[\frac{2\mu}{\hbar^2}\right]^{1/2}\int_{r_i}^{r_j}[E_{\rm c.m.}-U_{\rm eff}(r)]^{1/2} \times\left\{\frac{U''_{\rm eff}(r)g(r)-U'_{\rm eff}(r)g'(r)}{[U'_{\rm eff}(r)]^2}\right\}dr . \quad (13)$$

We have checked numerically on a particular example that (12) holds with very good accuracy for reasonable modifications of the original optical potential (i.e., changes of the order of a few MeV).

If we restrict to short-ranged perturbations $g(r)$ affecting only the internal action integral S_{32}, these will induce the following changes of the internal reflection coefficient η_I [cf. Eq. (7)]:

$$\eta_I\rightarrow\eta_I e^{2i\alpha\kappa} , \quad (14)$$

and the barrier wave reflection coefficient η_B will remain unaffected. Performing two modifications of this type will thus make it possible to separate the barrier and internal components η_B and η_I of the total reflection coefficient η. For example, if we perform three successive optical model calculations with the following potentials

$$V_{\rm opt}(r) , \quad (15a)$$

$$V_{\rm opt}(r)+\kappa_0 g(r) , \quad (15b)$$

$$V_{\rm opt}(r)-\kappa_0 g(r) , \quad (15c)$$

(where $V_{\rm opt}$ is the optical potential whose properties we want to investigate), the corresponding reflection coefficients will read

$$\eta^{(0)}=\eta_B+\eta_I , \quad (16a)$$

$$\eta^{(+)}=\eta_B+\eta_I e^{2i\alpha\kappa_0} , \quad (16b)$$

$$\eta^{(-)}=\eta_B+\eta_I e^{-2i\alpha\kappa_0} . \quad (16c)$$

Eliminating the complex constant α from this system and solving for η_B and η_I gives

$$\eta_B=\frac{\eta^{(+)}\eta^{(-)}-\eta^{(0)2}}{\eta^{(+)}+\eta^{(-)}-2\eta^{(0)}}\ ,\quad \eta_I=\eta^{(0)}-\eta_B\ . \tag{17}$$

This can be written in terms of the differences $\Delta^{(\pm)}\equiv(\eta^{(\pm)}-\eta^{(0)})$ as

$$\eta_B=\eta^{(0)}+\frac{\Delta^{(+)}\Delta^{(-)}}{\Delta^{(+)}+\Delta^{(-)}}\ ,\quad \eta_I=-\frac{\Delta^{(+)}\Delta^{(-)}}{\Delta^{(+)}+\Delta^{(-)}}\ . \tag{18}$$

III. NUMERICAL EVALUATION OF THE BARRIER AND INTERNAL WAVE AMPLITUDES

We now turn to the practical use of the approach presented in the preceding section. It should be recalled that our method, which is based on the semiclassical decomposition of Eq. (7), makes sense only if the real part of the effective potential $U_{\rm eff}$ has a well marked pocket for all the active partial waves (i.e., those for which $E_{\rm c.m.}\gtrsim V_B$), as is the case in the semiclassical approach. Moreover, the absorptive part W of the potential investigated must be strong enough to guarantee the absence of shape resonances, so that (7) is a good approximation to (4). Finally, there should not be more than three active turning points in the problem studied. Additional turning points[5] can be expected to appear for imaginary potentials with a very small diffuseness (that is, for $a_W\lesssim 0.3$ fm) or in the case of nonmonotonic, rapidly varying real potentials.

Although the method could be worked out with modifications of a different type, we decided to restrict to imaginary perturbations, i.e.,

$$\kappa g(r)=\pm iW_1 h(r)\ , \tag{19}$$

where W_1 is a real constant. The real perturbing form factor $h(r)$ should display two essential features: (i) it has to decrease fast enough at large r not to modify the barrier wave, and (ii) this decrease must be reasonably smooth so that it does not cause unwanted additional reflection inside the potential pocket. It was found that these conflicting constraints can be met with the following choice:

$$h(r)=\exp[-(r/\rho)^4]\ . \tag{20}$$

Numerical tests indicated that in order to satisfy condition (i) above the range ρ of the perturbation should be chosen as

$$\rho\approx R_B/2\ , \tag{21}$$

where R_B denotes the barrier radius (cf. Fig.1) for the grazing angular momentum. The amplitude W_1 of the perturbation should be reasonably small so that η_I behaves as indicated in (14). In practical calculations W_1 was chosen as

$$W_1\approx 0.1W_0\ , \tag{22}$$

where W_0 is the strength of the original imaginary potential. It must be stressed that the results generated by the proposed method can be considered meaningful only if they do not depend critically on the parameters of the perturbation ρ and W_1.

In Fig. 3, we present a detailed comparison of the barrier and internal components of the reflec-

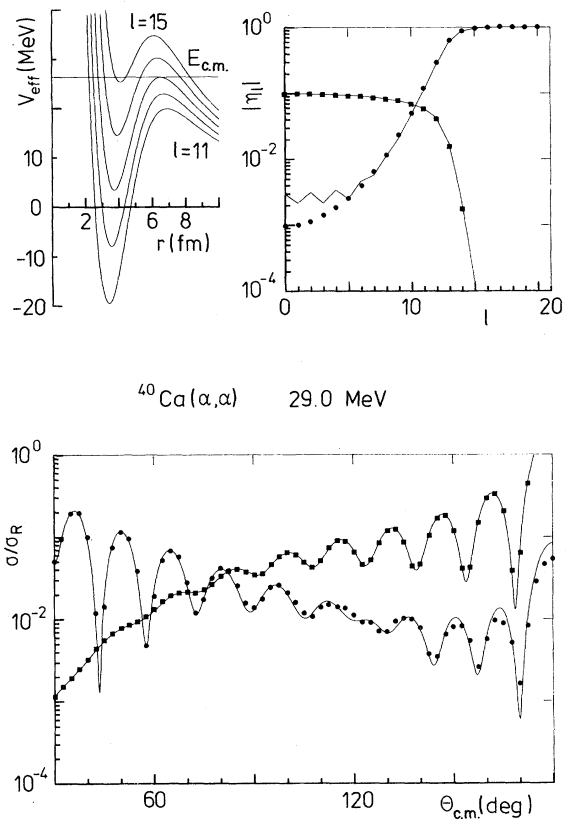

FIG. 3. ^{40}Ca(α,α) at 29.0 MeV laboratory energy (a) real part of the effective potential for angular momenta near the grazing; the horizontal line corresponds to the center of mass energy; (b) barrier and internal wave contributions to the scattering reflection coefficients (our method), full lines; WKB (barrier), dots; WKB (internal), squares; (c) same as (b) for the barrier and internal wave cross sections. The parameters of the modification used and those of the original potential can be found in Tables I and II.

tion coefficients and scattering cross sections generated by our method and by the semiclassical code[3] for $^{40}Ca(\alpha,\alpha)$ scattering at 29 MeV incident energy. The potential used in these calculations is that of Delbar *et al.*[6] The parameters of the modification and those of the investigated optical potential can be found in Tables I and II. Examination of Fig. 3 reveals a very good agreement between both methods, particularly for the internal wave contribution. For low angular momentum, however, there is a systematic discrepancy for the barrier wave reflection coefficients. Owing to the smallness of the latter, this is seen to have only limited impact on the corresponding cross section (cf. Fig. 3). We would like to point out in this respect that such a kind of decomposition is not intended to provide us with high accuracy results but rather with a semiquantitative understanding of the processes underlying the scattering. The origin of these small discrepancies is not fully understood. They seem to occur mainly when the internal wave contribution is large, i.e., for weak absorption. This makes us suspect that they are due to a very small residual resonant contribution to which our method, being based on the calculation of delicate differences, is expected to be particularly sensitive. This interpretation is substantiated by the success of the following variant of the method. We replace the perturbation of Eq. (19) with

$$\kappa g(r)=i(\pm W_1-W_2)h(r)\ , \tag{23}$$

where W_1 and $h(r)$ remain as defined above and W_2 is an extra positive constant which has to be chosen large enough to damp out the remaining resonant contribution. The magnitude of W_2 must, of course, remain reasonable to avoid producing the kind of spurious reflection we discussed in Sec. II. In practice, it can be chosen so that the modified internal wave reflection coefficients become comparable to the barrier ones for low angular momenta. Numerical tests indicated that the detailed choice of W_2 is still less stringent than that of the other parameters of the perturbation. Used with the modification (23) the method described at the end of Sec. II will now predict correctly only the barrier contribution η_B. The correct internal contribution η_I can be recovered by substracting these η_B from the reflection coefficients generated with the original potential without any modification. To summarize, using modification (23) thus requires four optical model evaluations corresponding to the following potentials [cf Eq. (15)]:

$$V_{\rm opt}(r)-iW_2h(r)\ , \tag{24a}$$

$$V_{\rm opt}(r)+i(W_1-W_2)h(r)\ , \tag{24b}$$

$$V_{\rm opt}(r)+i(-W_1-W_2)h(r)\ , \tag{24c}$$

$$V_{\rm opt}(r)\ . \tag{24d}$$

This new prescription leads to a much better agreement with the semiclassical approach, as can be seen in Fig. 4, where calculations were repeated for the same system as that studied in Fig. 3. Prescription (24) has been used for all the examples presented in the next section, although the simpler prescription (15) was found to provide reasonable results for all the investigated cases.

IV. APPLICATION OF THE METHOD TO LIGHT- AND HEAVY-ION SCATTERING

In this section we test our method against the semiclassical results for a few selected examples

TABLE I. Parameters of the modifications [Eqs. (19)—(23)] used to separate the various optical model scattering amplitudes into their barrier and internal components.

Case No.	System	$E_{\rm lab}$ (MeV)	ρ (fm)	W_1 (MeV)	W_2 (MeV)	Fig. No.
1	$\alpha+^{40}Ca$	29.0	3.25	1.0	0.0	3
2	$\alpha+^{40}Ca$	29.0	3.25	1.0	50.0	4
3	$\alpha+^{44}Ca$	29.0	3.40	2.0	20.0	5
4	$\alpha+^{90}Zr$	23.4	4.10	2.5	0.0	6
5	$^{6}Li+^{16}O$	29.8	2.70	0.7	30.0	7
6	$^{16}O+^{40}Ca$	54.0	4.50	1.0	20.0	8
7	$^{12}C+^{40}Ca$	51.0	4.10	1.0	20.0	11
8	$^{12}C+^{48}Ca$	47.2	4.00	1.0	15.0	12
9	$^{16}O+^{28}Si$	55.0	4.15	1.0	30.0	13
10	$^{16}O+^{28}Si$	55.0	4.20	1.0	20.0	14
11	$^{16}O+^{40}Ca$	50.0	4.50	1.0	10.0	15

TABLE II. Parameters of the investigated potentials [Eq. (25)] (refer also to Table I). Energies are expressed in MeV, lengths in fm.

Case No.	V_0	R_V	a_V	ν_V	W_0	R_W	a_W	ν_W	R_C	Ref.
1,2	188.92	4.685	0.645	2.0	11.342	6.0	0.5	2.0	4.446	6
3[a]	162.63	5.013	0.625	2.0	28.10	5.475	0.5	2.0	4.589	6
4	230.5	5.647	0.554	1.0	23.5	5.647	0.554	1.0	5.647	7
5	187.0	2.646	0.890	1.0	6.6	6.073	0.54	1.0	6.300	8
6	111.87	7.25	0.478	1.0	9.89	7.08	0.56	1.0	7.25	10
7	60.5	6.91	0.518	1.0	8.87	7.09	0.707	1.0	6.91	12
8	58.8	6.74	0.574	1.0	10.0	7.22	0.817	1.0	6.74	12
9	160.0	6.566	0.490	1.0	10.0	6.847	0.490	1.0	7.223	18
10	75.21	6.865	0.493	1.0	8.5	6.704	0.1844	1.0	7.892	19
11	50.0	7.894	0.42	1.0	7.6	5.94	0.30	1.0	5.94	9

[a]Some of the parameters of this potential have been refitted to experiment.

and we discuss briefly the physics involved. For each case presented the parameters of the modification (23) and those of the investigated potentials are collected in Tables I and II. The optical potentials we use have the form

$$V(r)=-V_0\{1+\exp[(r-R_V)/(\nu_V a_V)]\}^{-\nu_V},$$
$$W(r)=-W_0\{1+\exp[(r-R_W)/(\nu_W a_W)]\}^{-\nu_W}, \tag{25}$$

and the Coulomb potential $V_C(r)$ corresponds to a uniformly charged sphere of radius R_C.

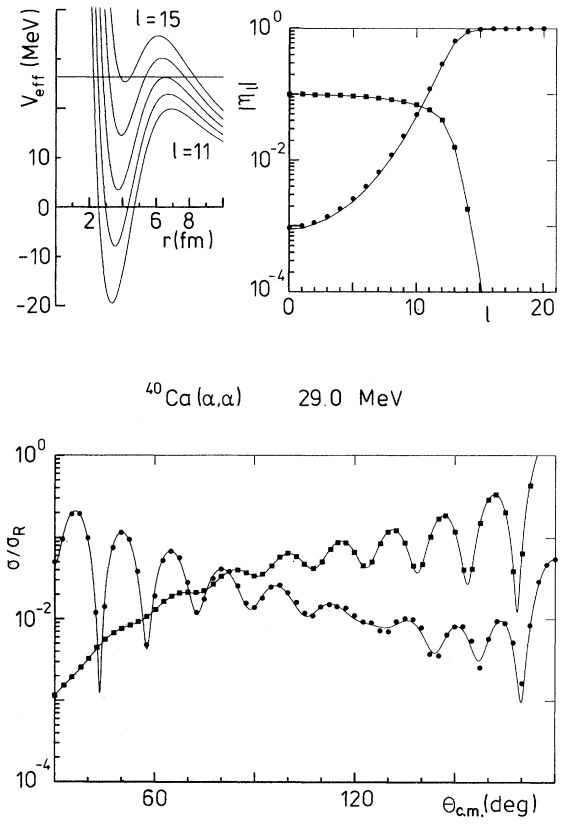

FIG. 4. Same as Fig. 3 for other parameters of the modification (see text and Table I).

A. ^{40,44}Ca(α,α) 29.0 MeV

Elastic α-particle scattering from the calcium isotopes has been thoroughly investigated because of the large backward enhancement seen in some experimental angular distributions (see, e.g., Ref. 6 and references quoted therein). The case of ^{40}Ca(α,α) at 29 MeV has been investigated in the preceding section. It can be seen in Fig. 4 that the internal wave contribution dominates at large angles and is responsible for the anomalous large angle scattering ("ALAS") observed for that system. We performed a similar decomposition for ^{44}Ca(α,α) at the same energy (see Fig. 5). Here the internal contribution is an order of magnitude smaller because of the stronger absorption, making the full scattering cross section look "normal." A detailed discussion of the semiclassical decomposition for these two systems can be found in Ref. 6.

B. ^{90}Zr(α,α) 23.4 MeV

This case has been selected because the excitation function around 175° displays a spectacular "dip," about 1 MeV wide, at about 23 MeV in-

cident energy.[7] Although these data (including the dip) could be fitted using a standard Woods-Saxon optical potential,[7] the particular features of the optical potential causing this dip were not understood. After carrying out the decomposition into barrier and internal components, it becomes clear that there is an accidental destructive interference between both components of the scattering amplitude which turn out to be of comparable magnitude for $\theta \approx 180°$ around this incident energy (cf. Fig. 6). A detailed calculation shows that they are, moreover, in phase opposition at the same energy. Our analysis thus reveals the purely accidental nature of the phenomenon; its occurrence is linked to a very unlikely coincidence between the detailed properties of the real and imaginary parts of the potential. Before we leave this case we would like to point to the very good agreement of the results of our method with those of the semiclassical approach.

C. $^{16}O(^{6}Li,^{6}Li)$ 29.8 MeV

The results obtained with the potential of Bassani *et al.*[8] are presented in Fig. 7. We observe an excellent agreement of the internal wave contributions generated by both decomposition methods. The agreement for the barrier wave contributions is not so good, although quite sufficient for our purpose.

The scattering is seen to be already dominated by the internal contribution at moderate angles as a result of the large values assumed by the corresponding reflection coefficients. The internal wave contribution is felt at angles as small as 50°. Our interpretation contrasts with that given in Ref. 8, where it was concluded that ^{6}Li behaves as a strongly absorbed projectile at low energy. The confusion seems to have originated from the presence of discrete ambiguities in the original optical model analysis. In fact, the discrete ambiguities evidenced in optical model analyses of elastic scattering data are in no way connected to the strong absorption properties of the interaction but can even appear for very weakly absorbing potentials, provided that the real part of the effective potential displays a pocket. Such potentials have

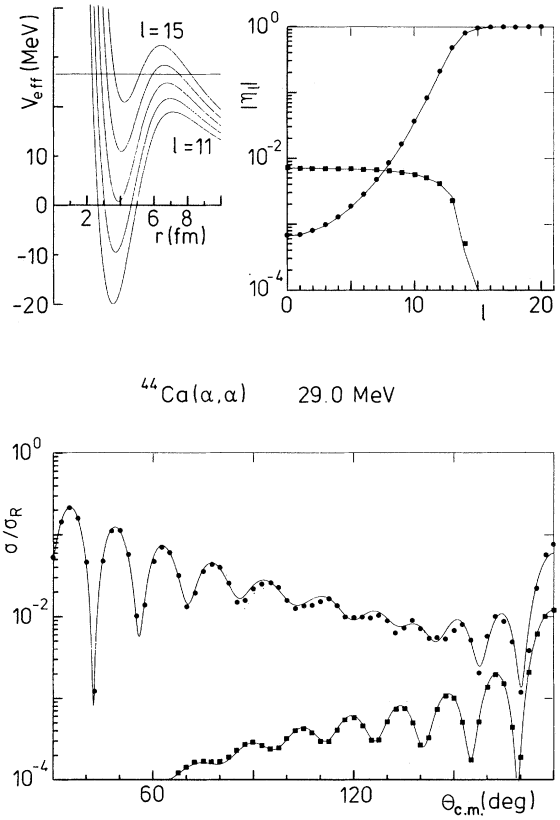

FIG. 5. Same as Fig. 3 for $^{44}Ca(\alpha,\alpha)$ at 29.0 MeV.

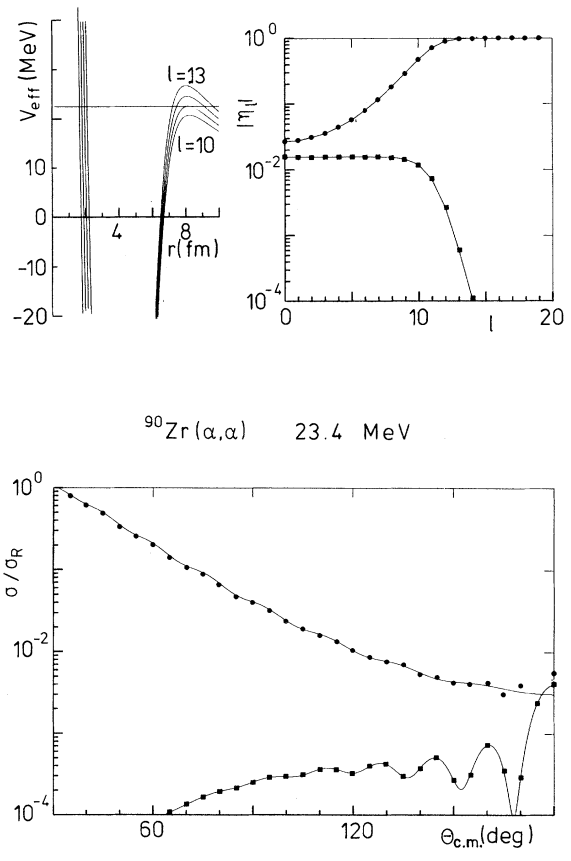

FIG. 6. Same as Fig. 3 for $^{90}Zr(\alpha,\alpha)$ at 23.4 MeV.

only to be connected by some set of conditions[2] to lead to the same scattering cross sections.

D. $^{40}Ca(^{16}O,^{16}O)$ 54.0 MeV

This system has been studied recently by Brookhaven[9] and Saclay[10] groups. An attractive feature of the measured cross sections is the occurrence of ALAS together with that of pronounced oscillations in the excitation function measured at 180°.[9] We compare the result of our decomposition against WKB for the potential of Ref. 10 in Fig. 8.

Here the internal contribution becomes important for angles larger than about 120°; both methods are in perfect agreement. The barrier contributions agree reasonably well up to about the same angle. For larger angles high frequency oscillations set in, in the WKB cross sections. These seem to originate from the bad convergence properties of the WKB reflection coefficients at large angular momenta. This phenomenon, which is not apparent in Fig. 8, is displayed in Fig. 9 on an expanded scale for large l values, where the internal contribution has become completely negligible. The WKB total reflection coefficients are seen to be systematically smaller than their quantum counterparts. This behavior introduces small spurious high l components in the scattering amplitude. This is expected to cause unphysical oscillations in the cases where the barrier cross section becomes very small (i.e., mainly for heavy-ion scattering where its ratio to Rutherford scattering falls to $10^{-5}-10^{-6}$ at large angles). An additional indication of the failure of WKB in this case is that the total WKB cross section is in bad disagreement with the quantum result at large angles (cf. Fig. 10). The sum of our barrier and internal wave amplitudes equals by definition the full quantum result; moreover our internal wave contribution is nearly identical to that generated by WKB and both internal and barrier contributions are of comparable magnitude at large angles in the present case. We thus have strong support to conclude that the barrier wave contribution given by our method is the correct one. In Fig. 8 and the fol-

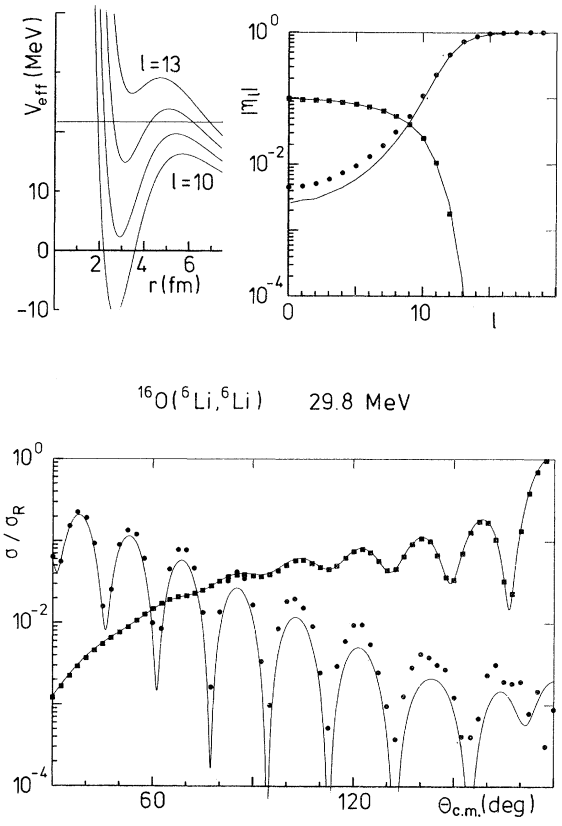

FIG. 7. Same as Fig. 3 for $^{16}O(^6Li,^6Li)$ at 29.8 MeV.

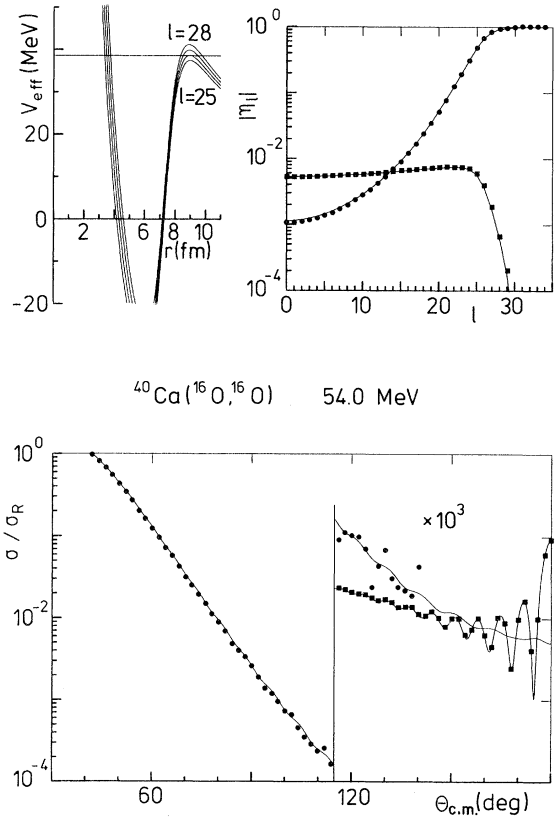

FIG. 8. Same as Fig. 3 for $^{40}Ca(^{16}O,^{16}O)$ at 54.0 MeV.

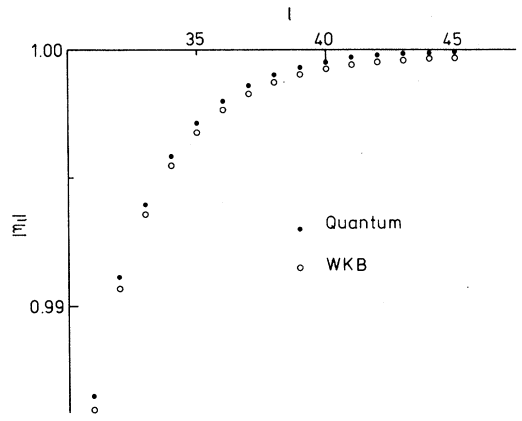

FIG. 9. Comparison of the modulus of the quantum and WKB reflection coefficients at large l for case No. 6.

lowing figures, the WKB barrier cross section has therefore only been displayed for angles where it is thought to be meaningful.

As in the present case the barrier and internal contributions are of comparable size at large angles they strongly interfere making the total scattering cross section very sensititve to small changes in both incident energy and optical potential parameters. This interference between both components of the scattering amplitude could account for the broad oscillatory structure seen in the experimental excitation function at 180°,[9] as proved to be the case for low-energy α-particle scattering from ^{40}Ca.[11]

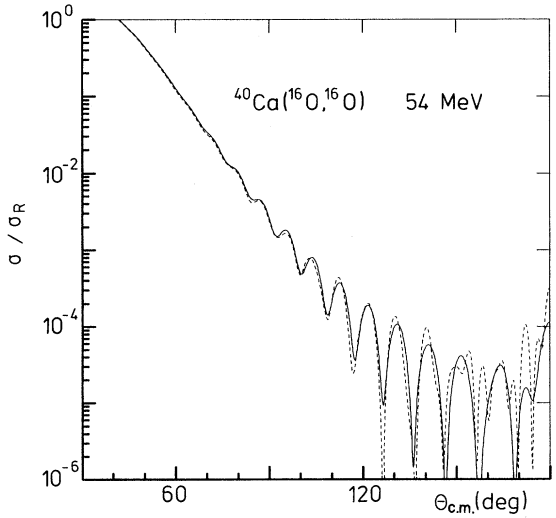

FIG. 10. Comparison of the full quantum (full line) and WKB (dotted line) cross sections for case No. 6.

E. ^{40}Ca(^{12}C,^{12}C) 51 MeV and ^{48}Ca(^{12}C,^{12}C) 47.2 MeV

A clear-cut isotopic effect has recently been observed for these two systems by Renner[12] at forward angles ($\theta_{c.m.} < 105°$). The elastic scattering angular distribution displays well marked oscillations in the case of ^{40}Ca, while it shows a nearly exponential falloff for ^{48}Ca. Both angular distributions could be fitted with conventional Woods-Saxon potentials.[12] In Figs. 11 and 12 are presented the decompositions we carried out for both systems.

In the case of ^{40}Ca(^{12}C,^{12}C) we observe the presence of oscillations in the barrier cross section already at forward angles. The internal wave contribution dominates the scattering for angles exceeding about 110°. For smaller angles its influence can be felt in the total cross section in that it enhances the amplitude of the oscillations seen in the barrier part. Both contributions are thus material in reproducing the oscillatory structure of the data.

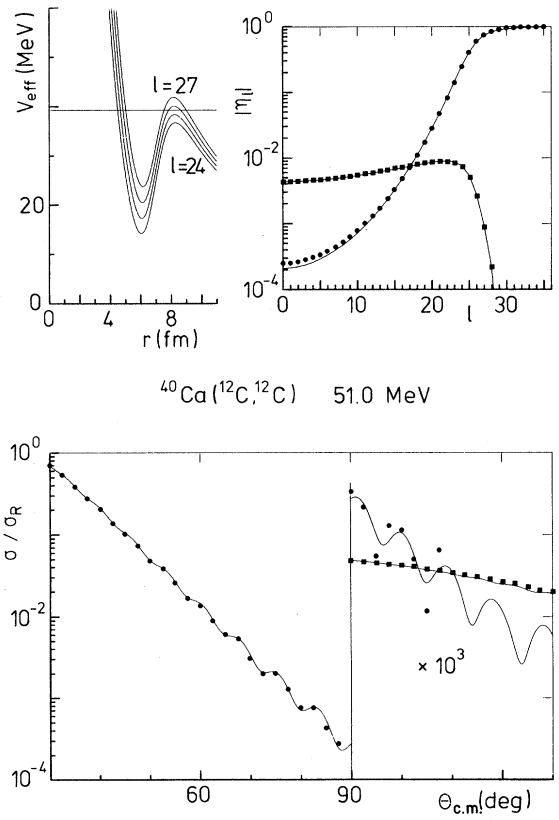

FIG. 11. Same as Fig. 3 for ^{40}Ca(^{12}C,^{12}C) at 51.0 MeV.

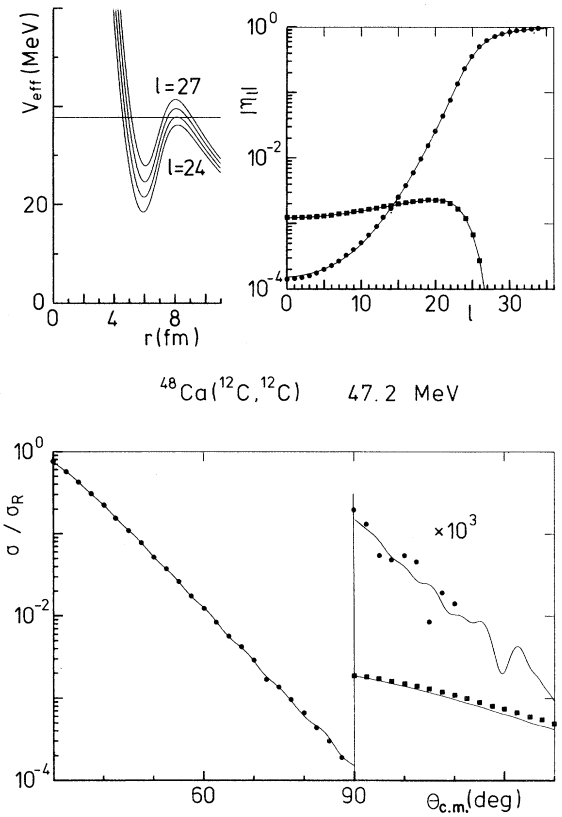

FIG. 12. Same as Fig. 3 for ^{48}Ca(^{12}C,^{12}C) at 47.2 MeV.

On the other hand, the barrier part of ^{48}Ca(^{12}C,^{12}C) scattering is much smoother than its ^{40}Ca counterpart. Moreover, the internal contribution for ^{48}Ca is very similar in shape to that observed for ^{40}Ca but an order of magnitude smaller. In the experimentally investigated angular range it is negligible and the total elastic scattering cross section remains smooth.

In order to ascertain the origin of the oscillations seen in the barrier part of ^{40}Ca(^{12}C,^{12}C) scattering, we repeated the calculations for ^{48}Ca using the ^{40}Ca absorption. Oscillations appeared in the resulting barrier contribution, although of much smaller amplitude than those evidenced in the former case. The difference of behavior seen in elastic scattering from ^{40}Ca and ^{48}Ca is thus due not only to a difference in absorption but also to some extent to a difference in the real parts of the effective potentials in their surface region.

The ^{40}Ca(^{12}C,^{12}C) excitation function measured at back angles[13] displays broad oscillations, a few MeV wide. Oscillations of comparable width are automatically generated by the optical potential adjusted to the forward angle data. A semiclassical estimate of multiple reflection rules out an interpretation of these structures in terms of shape resonances, as absorption turns out to be too strong. They rather can be viewed as due to the variation with energy of the state of interference of the barrier and internal wave contributions, as discussed in the preceding subsection for the ^{40}Ca(^{16}O,^{16}O) case.

F. ^{28}Si(^{16}O,^{16}O) 55 MeV

This is the first heavy-ion system for which ALAS was observed experimentally.[14,15] The data have been fitted to various degrees of accuracy using several optical model potentials.[16–19] Some of these potentials have been investigated within the semiclassical approach be Lee.[19] In Fig. 13 we present the results of our method for the potential proposed by Terenetski and Garrett[18] which fulfills all the requirements discussed in Sec. III. As discussed in Ref. 18, the backward angle scattering is dominated by the internal wave contribution which exceeds the barrier one by up to two orders of magnitude, and is entirely responsible for ALAS. The other potentials investigated by Lee were shown to contain essentially the same physical picture. Also it was shown in that paper[19] that the oscillatory structure of the experimental backward angle excitation function could be understood as the result of the interference between both components of the scattering amplitude.

G. Borderline cases

In this final subsection, we investigate two cases for which some of the conditions of applicability of our method, which were enumerated in Sec. III, are *not* met.

The first example we present is again that of ^{28}Si(^{16}O,^{16}O) scattering at 55 MeV incident energy but we now consider the optical potential proposed by Golin and Kahana.[19] This potential satisfies all the requirements expressed in Sec. III, except that it has a very small imaginary diffuseness $a_W = 0.1844$ fm. Therefore the semiclassical description of the problem involves four active turning points[19] due to the reflection now taking place at the sharp imaginary potential surface. The imaginary radius ($R_w = 6.704$ fm) is somewhat smaller than the barrier radius ($R_B \approx 8.4$ fm) making this potential slightly surface transparent. Comparison of our decomposition with that

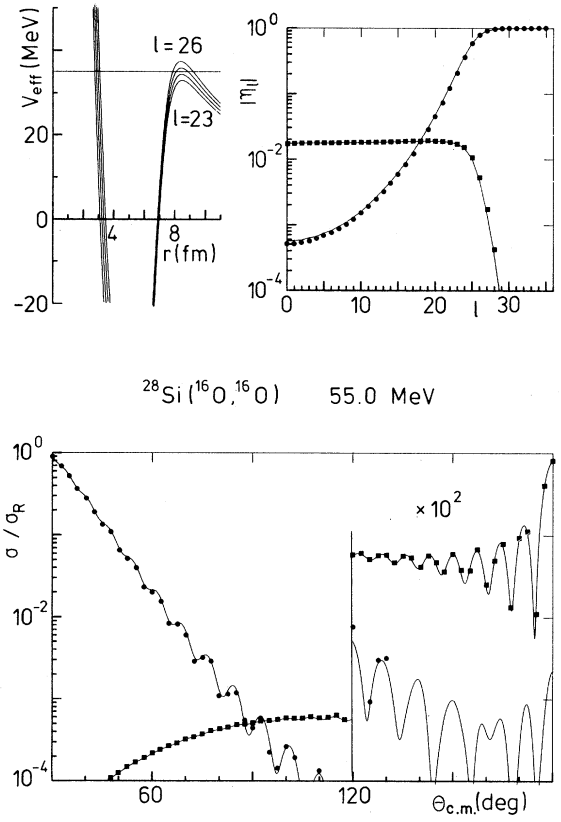

FIG. 13. Same as Fig. 3 for ^{28}Si(^{16}O,^{16}O) at 55.0 MeV [Terenetski and Garrett potential (Ref. 18)].

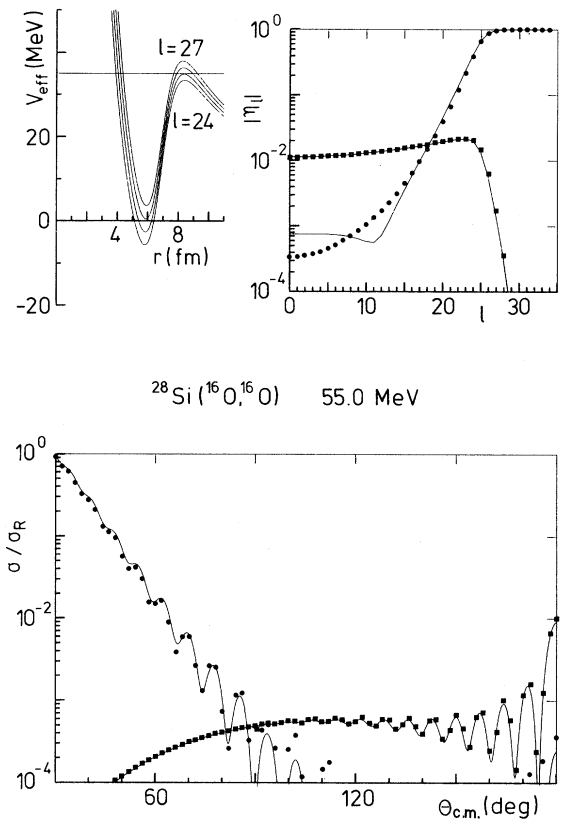

FIG. 14. Same as Fig. 3 for ^{28}Si(^{16}O,^{16}O) at 55.0 MeV [Golin and Kahana potential (Ref. 19)].

predicted by the three-turning point semiclassical code[3] is displayed in Fig. 14. Both methods are seen to be in very good agreement for the internal wave reflection coefficients and scattering cross sections, but the barrier wave reflection coefficients disagree badly for low angular momentum. However, the barrier wave angular distributions are in reasonable agreement in the angular range where they are physically important (i.e., not dominated by the internal wave contribution). This result is consistent with the conclusion of Lee[19] that reflection at the imaginary barrier is of minor importance to the present scattering process. Returning to the detailed derivation of our approach (Sec. III), one sees that our calculations are expected to give a correct internal wave contribution and provide us, in lieu of the correct barrier wave contribution, with the sum of the barrier contribution and that corresponding to reflection at the imaginary surface, because the range (21) of our modification is less than the imaginary radius. On the other hand, the three-turning point semiclassical approach is expected to give a less precise description of the physics involved since it completely neglects the reflectivity of the imaginary potential; this defect can only be remedied by having recourse to a more elaborate multiturning point approach.[5,19] To summarize we can conclude that our method can still give useful information about the scattering mechanism even in the case of imaginary potentials with very small diffusenesses provided the imaginary radius is not too small (which may lead to high surface transparency, see below) and at the expense of a reinterpretation of the barrier wave contribution supplied by the method.

The second example we choose to illustrate the pitfalls associated with the use of our method for potentials not satisfying the criteria of Sec. III, is that of ^{40}Ca(^{16}O,^{16}O) scattering at 50 MeV incident energy. The optical potential we investigate is that of Kubono *et al.*[9] (ST2). This interaction has a small imaginary diffuseness ($a_W = 0.3$ fm), but also an imaginary radius ($R_W = 5.94$ fm) much smaller than the barrier radius ($R_B \approx 9$ fm). These two properties make this potential very weakly absorbing near the grazing angular momentum (cf.

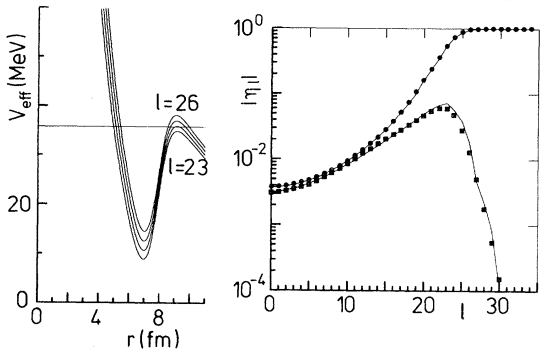

FIG. 15. Same as Fig. 3 for ^{40}Ca(^{16}O,^{16}O) at 50.0 Mev [Kubono *et al.* ST2 potential (Ref. 9), effective potential and reflection coefficients only].

Fig 15), i.e., it is highly surface transparent (hence its name). In this case we can expect the occurrence of resonances (i.e., multiple reflection) at high angular momentum, which we neglected completely in the derivation of our method. Comparison of the reflection coefficients calculated by means of the semiclassical code according to formula (4) and its approximation (7) confirms the existence of important resonant contributions for $l \gtrsim 20$. The internal reflection coefficients generated by both methods can be seen to disagree systematically in this domain of angular momenta (Fig. 15). This discrepancy has a dramatic impact on the corresponding cross sections which are in complete disagreement at back angles (our method predicts large spurious oscillations in the internal wave cross section). Although a careful inspection of the potential parameters could have revealed its inadequacy for the application of our decomposition method, it is a simple matter to detect the type of spurious results discussed here. We stressed in Sec. III that the result should not depend critically on the parameters of the perturbation used (except perhaps for the smaller of the two components when it is much smaller than the other). This consistency condition turns out to be violated in the present case, as calculations repeated with different values of, e.g., W_2 lead to quite different results for the internal wave cross section (Fig. 16). This type of instability was never observed for any of the cases presented in the preceding subsections, nor for the first example of the present one. For example, calculations similar to those presented in Fig. 16, repeated for the case of subsection *D*, i.e., ^{40}Ca(^{16}O,^{16}O) at 54.0 MeV, lead to curves which are indistinguishable at the scale of the figure — and in very good agreement with WKB as was shown in Fig. 8.

V. SUMMARY AND CONCLUSIONS

In this paper we have presented a new technique for decomposing the light- and heavy-ion elastic scattering amplitude into its barrier and internal wave components. Contrary to the original semiclassical approach developed by Brink and Takigawa[2] for that purpose, our method requires only minimum programming as it makes use of the re-

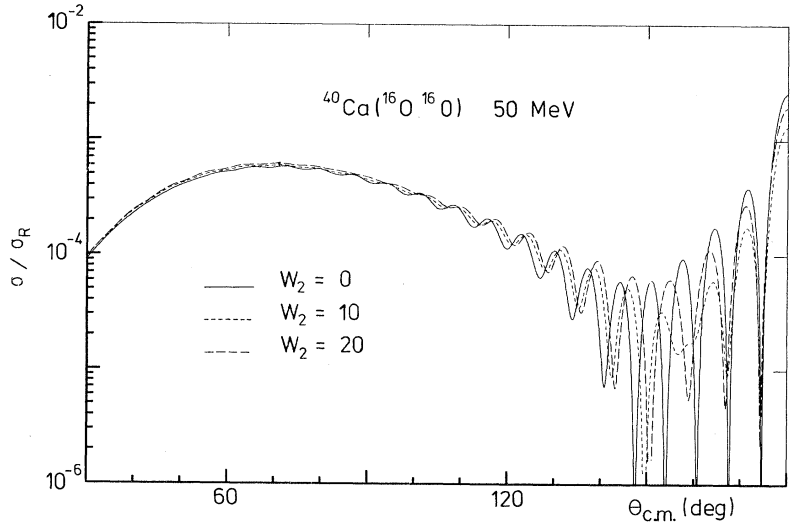

FIG. 16. Behavior of the internal wave contribution generated by our method for different values of the parameter W_2 [cf. Eq. (23)] (case No. 11).

flection coefficients generated by any standard optical model code. The very good agreement observed between our method and the semiclassical results also makes it a promising tool for investigating cases which are out of reach of the semiclassical approach, e.g., folding model, "model independent," and numerically-supplied potentials.

The physical interest of this type of decomposition has been illustrated by applying our method to a few selected examples — most of which were not investigated previously from the present point of view — ranging from α- to heavy-ion scattering.

ACKNOWLEDGMENTS

One of the authors (F.M.) acknowledges useful discussions with Professor C. Marty and Dr. N. Takigawa at the early stage of this work. The other (J.A.) is grateful to Professor R. Ceuleneer for having made possible his stay at the University of Mons, and to IISN for financial support. Both are very indebted to Professor R. Ceuleneer for his constant help and interest and for his careful reading of our manuscript, and to Dr. G. Reidemeister for illuminating discussions.

---

*Permanent address: Institute of Nuclear Physics, 31-342 Cracow, Poland.

[1]R. Schaeffer, in *Theoretical Methods in Medium-Energy and Heavy-ion Physics,* edited by K. W. McVoy and W. A. Friedman (Plenum, New York, 1978), p.189.

[2]D. M. Brink and N. Takigawa, Nucl. Phys. A279, 159 (1977).

[3]R. Vanderpoorten, code KGB2, Université de l'Etat à Mons, Belgium (unpublished).

[4]N. Rowley, H. Doubre, and C. Marty, Phys. Lett. 69B, 147 (1977).

[5]S. Y. Lee and N. Takigawa, Nucl. Phys. A308, 189 (1978).

[6]T. Delbar, G. Grégoire, G. Paic, R. Ceuleneer, F. Michel, R. Vanderpoorten, A. Budzanowski, H. Dabrowski, L. Freindl, K. Grotowski, S. Micek, R. Planeta, A. Strzalkowski, and K. A. Eberhard, Phys. Rev. C 18, 1237 (1978).

[7]M. Wit, J. Schiele, K. A. Eberhard, and J. P. Schiffer, Phys. Rev. C 12, 1447 (1975).

[8]G. Bassani, N. Saunier, B. M. Traore, J. Raynal, A. Foti, and G. Pappalardo, Nucl. Phys. A189, 353 (1972).

[9]S. Kubono, P. D. Bond, and C. E. Thorn, Phys. Lett. 81B, 140 (1979).

[10]N. Alamanos, M. Lamehi-Rachti, C. Lévi, L. Papineau, and P. Talon, Nucl. Phys. A363, 477 (1981).

[11]S. Y. Lee, N. Takigawa, and C. Marty, Nucl. Phys. A308, 161 (1978).

[12]T. R. Renner, Phys. Rev. C 19, 765 (1979).

[13]T. R. Renner, J. P. Schiffer, D. Horn, G. C. Ball, and W. G. Davies, Phys. Rev. C 18, 1927 (1978).

[14]P. Braun-Munziger, G. M. Berkowitz, T. M. Cormier, C. M. Jachcinski, J. W. Harris, J. Barrette, and M. J. Le Vine, Phys. Rev. Lett. 38, 944 (1977).

[15]J. Barrette, M. J. Le Vine, P. Braun-Munziger, G. M. Berkowitz, M. Gai, J. W. Harris, C. M. Jachcinski, Phys. Rev. Lett. 40, 445 (1978).

[16]D. Dehnhard, V. Shkolnik, and M. A. Franey, Phys. Rev. Lett. 40, 1549 (1978).

[17]V. Shkolnik, M. A. Franey, and D. Dehnhard, Proceedings of the International Conference on Nuclear Physics, Berkeley, 1980 (unpublished), Vol. I, p. 588.

[18]K. O. Terenetski and J. D. Garrett, Phys. Rev. C 18, 1944 (1978).

[19]S. Y. Lee, Nucl. Phys. A311, 518 (1978).